

Quenched lattice calculation of the vector channel $B \rightarrow D^* \ell \nu$ decay rate

G.M. de Divitiis^{a,b}, R. Petronzio^{a,b}, N. Tantalo^{b,c}

^a *Università di Roma “Tor Vergata”, I-00133 Rome, Italy*

^b *INFN sezione di Roma “Tor Vergata”, I-00133 Rome, Italy*

^c *Centro Enrico Fermi, I-00184 Rome, Italy*

We calculate, in the continuum limit of quenched lattice QCD, the form factor that enters the decay rate of the semileptonic decay $B \rightarrow D^* \ell \nu$. By using the step scaling method (SSM), previously introduced to handle two scale problems in lattice QCD, and by adopting flavor twisted boundary conditions we extract $F^{B \rightarrow D^*}(w)$ at finite momentum transfer ($w \geq 1$) and at the physical values of the heavy quark masses. Our results can be used in order to extract the CKM matrix element V_{cb} by the experimental decay rate without model dependent extrapolations. The value of V_{cb} agrees with the one obtained from the $B \rightarrow D \ell \nu$ channel and makes us confident that the quenched approximation well applies to these transitions.

I. INTRODUCTION

Physics beyond the Standard Model may show up in the hadronic flavor sector of the theory and could be revealed by measuring independently the different entries of the Cabibbo–Kobayashi–Maskawa [1, 2] matrix and by looking for deviations from unitarity (unitarity triangle analysis, UTA) [3]. On the theoretical side, a percent relative accuracy on the hadronic matrix elements entering the different variants of the UTA’s [4] is needed and lattice QCD calculations may eventually provide the required non-perturbative precision. The study of semileptonic decays of heavy-light mesons mediated by flavor changing $\Delta F = 1$ hadronic currents gives direct access to CKM matrix elements and is particularly convenient from the point of view of lattice QCD calculations. The form factors entering the decay rates are dimensionless quantities and do not inherit uncertainties from the scale setting procedure. Moreover they can be expressed in terms of matrix elements undergoing finite and multiplicative renormalization and symmetry arguments can be used to constrain numerical results (Ademollo–Gatto theorem, Luke’s theorem, spin-symmetry in the heavy quark limit). Finally, matrix elements involve a single hadron both in initial and final states thus avoiding complications due to final state interactions.

In two previous papers [5, 6] we have calculated, in the quenched approximation of QCD, the form factors entering the decay rate of the process $B \rightarrow D \ell \nu$ at non vanishing momentum transfer and, comparing with experiment, we have extracted the CKM matrix element V_{cb} . In this work we extend our quenched study of heavy-light mesons semileptonic decays by calculating the form factors entering the decay rate for the process $B \rightarrow D^* \ell \nu$. At vanishing momentum transfer the study of pseudoscalar to vector semileptonic transitions requires the calculation of a single form factor with respect to the two required in the case of pseudoscalar to pseudoscalar transitions. At finite momentum transfer the study of pseudoscalar-vector transitions requires the calculation of a particular linear combination of four

different form factors, $F^{B \rightarrow D^*}(w)$. Here we compute $F^{B \rightarrow D^*}(w)$ in the interval $1 \leq w = v_B \cdot v_{D^*} \leq 1.1$ thus allowing the extraction of V_{cb} without extrapolating experimental data to zero recoil. Although in this case the extrapolation is much less dramatic than in the pseudoscalar-pseudoscalar channel an important source of systematics can be avoided by using our results.

As in refs. [5, 6] we make use of the Step Scaling Method [7] devised to reconcile large quark masses with adequate lattice resolution and large physical volumes and successfully applied also to the determination of heavy quark masses and decay constants [8, 9, 10]. We obtain results at non zero momentum transfer with good accuracy by enforcing special boundary conditions on the quark fields, called flavor twisted [11], that shift by an arbitrary amount the discretized set of lattice momenta (see also [12, 13, 14]).

Our results are not the final ones since they have been obtained within the quenched approximation. Quenching introduces a systematic error that it is hard to quantify (if not impossible) but allows us, in view of a future unquenched calculation, to check all the remaining systematics (heavy quark methodology, continuum and chiral limits, etc.) and to discuss some technical issues related to the choice of interpolation operators for vector mesons carrying non vanishing spatial momenta to be used within the Schrödinger Functional formulation of lattice QCD. Furthermore precise results for $F^{B \rightarrow D^*}(w)$ at $w > 1$ are presently missing even in the quenched approximation.

To estimate the validity of the quenched approximation we calculate the ratio of physical decay rates between vector and pseudoscalar final states. This ratio is indeed a purely QCD observable, independent from the value of V_{cb} , and can be directly compared with experiment. Our results agree with the measured ratio within experimental errors thus indicating that residual unquenched corrections are likely within the current experimental uncertainties.

II. FORM FACTORS AND DECAY RATE

The semileptonic decay of a pseudoscalar meson into a vector meson is mediated by the weak $\mathcal{V}-\mathcal{A}$ current. The relevant matrix elements can be parametrized in terms of four form factors. Among possible parameterizations we choose the following one

$$\begin{aligned} \frac{\langle \mathcal{M}_V^\alpha | \mathcal{V}^\mu | \mathcal{M}_P \rangle}{\sqrt{M_V M_P}} &= \varepsilon^{\mu\nu\rho\sigma} v_P^\nu v_V^\rho \epsilon_\alpha^{*\sigma} h_V \\ \frac{\langle \mathcal{M}_V^\alpha | \mathcal{A}^\mu | \mathcal{M}_P \rangle}{\sqrt{M_V M_P}} &= \\ &= i \epsilon_\alpha^{*\nu} [h_{A_1}(1+w)g^{\mu\nu} - (h_{A_2}v_P^\mu + h_{A_3}v_V^\mu)v_P^\nu] \end{aligned} \quad (1)$$

where we have used the greek letters μ, ν, ρ, σ to indicate Lorentz indices, $M_{P,V}$ are the masses of the pseudoscalar (\mathcal{M}_P) and vector (\mathcal{M}_V^α) mesons, $v_{P,V} = p_{P,V}/M_{P,V}$ their 4-velocities, $\varepsilon^{\mu\nu\rho\sigma}$ is the totally antisymmetric tensor in four dimensions ($\varepsilon^{0123} = 1$) while ϵ_α^μ is the polarization vector of \mathcal{M}_V^α ,

$$\sum_{\alpha=1}^3 \epsilon_\alpha^{*\mu} \epsilon_\alpha^\nu = T^{\mu\nu} = -g^{\mu\nu} + v_V^\mu v_V^\nu \quad (2)$$

The form factors depend upon the masses of the initial and final particles and upon $w \equiv v_V \cdot v_P$

$$\begin{aligned} h_{V,A_i} &\equiv h_{V,A_i}^{P \rightarrow V}(w) \equiv h_{V,A_i}(w, M_P, M_V) \\ 1 \leq w &\leq (M_P^2 + M_V^2)/2M_P M_V \end{aligned} \quad (3)$$

In the case where M_P is the B meson mass and M_V is the D^* meson mass the maximum value of w is around 1.5.

The differential decay rate of the process $B \rightarrow D^* \ell \nu$, in the case of massless leptons, is given by

$$\begin{aligned} \frac{d\Gamma^{B \rightarrow D^* \ell \nu}}{dw} &= |V_{cb}|^2 \frac{G_F^2}{48\pi^3} M_B^5 (1-r)^2 r^3 \times \\ &\sqrt{w^2 - 1} (1+w)^2 \lambda(w) \left[F^{B \rightarrow D^*}(w) \right]^2 \end{aligned} \quad (4)$$

where we have defined $r = M_V/M_P$ and

$$\begin{aligned} t^2(w) &= \frac{1 - 2wr + r^2}{(1-r)^2} \\ \lambda(w) &= 1 + \frac{4w}{w+1} t^2(w) \end{aligned} \quad (5)$$

The function $F^{B \rightarrow D^*}(w)$,

$$F^{B \rightarrow D^*}(w) = h_{A_1}(w) \sqrt{\frac{H_0^2(w) + H_+^2(w) + H_-^2(w)}{\lambda(w)}} \quad (6)$$

with

$$\begin{aligned} X_V(w) &= \sqrt{\frac{w-1}{w+1}} \frac{h_V(w)}{h_{A_1}(w)} \\ X_2(w) &= (w-1) \frac{h_{A_2}(w)}{h_{A_1}(w)} \\ X_3(w) &= (w-1) \frac{h_{A_3}(w)}{h_{A_1}(w)} \\ H_0(w) &= \frac{w-r - X_3(w) - rX_2(w)}{1-r} \\ H_\pm(w) &= t(w) [1 \mp X_V(w)] \end{aligned} \quad (7)$$

is the non perturbative input needed to extract V_{cb} by the measurement of the decay rate.

By noting that at zero recoil $F^{B \rightarrow D^*}(1)$ is identically equal to $h_{A_1}(1)$ the complexity of the theoretical calculation can be considerably reduced since, in this particular case, a single matrix element with initial and final particles both at rest is needed instead of the four matrix elements at non vanishing momentum transfer required to solve the full system of eqs. (1) with respect to h_{V,A_i} . For these reasons previous lattice studies have been devoted to the calculation of $F^{B \rightarrow D^*}(w)$ at zero recoil only, where it can be extracted with good statistical accuracy both in the quenched approximation [16] and in the $n_f = 2 + 1$ unquenched theory [15]. On the other hand, it is not possible to measure directly the decay rate at zero recoil because of the presence of the kinematical factor $(w-1)^{1/2}$ in eq. (4) and experimental data at $w = 1$ are obtained by extrapolation. The systematics introduced by this extrapolation is much less dramatic with respect to the case of the decay $B \rightarrow D \ell \nu$ where the kinematical suppression goes like $(w-1)^{3/2}$ but can be nevertheless eliminated. In the following we calculate $F^{B \rightarrow D^*}(w)$ in the range $1 \leq w \leq 1.1$ that includes values of w where experimental data are directly available with good precision.

III. SCHRÖDINGER FUNCTIONAL CORRELATORS

We have carried out the calculation within the $O(a)$ improved Schrödinger Functional formalism [17, 18]

with vanishing background fields. The choice of the Schrödinger Functional regularization is particularly convenient to perform simulations on small physical volumes (see section IV) because Dirichlet boundary conditions in the time direction provide an infrared regulator that allows the simulation of massless quarks. At the same time, the extraction of physical matrix elements involving vector mesons at non vanishing spatial momenta from Schrödinger Functional correlators requires some additional care with respect to the case of quark fields satisfying periodic boundary conditions in the time direction.

A. Boundary and bulk operators

In defining interpolation operators of meson states we need to distinguish between bulk fields $\psi(x)$, boundary fields $\zeta(x)$ living at $x_0 = 0$

$$\begin{aligned} P_+ \zeta(\vec{x}) &= \frac{1 + \gamma_0}{2} \psi(0, \vec{x}) = 0 \\ \bar{\zeta}(\vec{x}) P_- &= \bar{\psi}(0, \vec{x}) \frac{1 - \gamma_0}{2} = 0 \end{aligned} \quad (8)$$

and boundary fields $\zeta'(x)$ living at $x_0 = T$

$$\begin{aligned} P_- \zeta'(\vec{x}) &= \frac{1 - \gamma_0}{2} \psi(T, \vec{x}) = 0 \\ \bar{\zeta}'(\vec{x}) P_+ &= \bar{\psi}(T, \vec{x}) \frac{1 + \gamma_0}{2} = 0 \end{aligned} \quad (9)$$

Different quark flavors will be distinguished, if needed, by using explicit indexes. External momenta have been set by using flavor twisted b.c. for the heavy flavors. In particular we have used

$$\begin{aligned} \psi(x + \hat{1}L) &= e^{i\theta} \psi(x) \\ p_1 &= \frac{\theta}{L} + \frac{2\pi k_1}{L}, \quad k_1 \in \mathbb{N} \end{aligned} \quad (10)$$

with different values of θ for the different heavy quarks and ordinary periodic b.c. in the other spatial directions and for the light quarks.

A generic meson state on the boundaries can be expressed as a bilinear field operator acting on the vacuum. In the case of vector mesons, the Schrödinger Functional boundary conditions select a particular combination between the two possible choices $V^\mu(x) = \bar{\psi}(x)\gamma^\mu\psi(x)$ and $T^{0\mu}(x) = \bar{\psi}(x)\gamma^0\gamma^\mu\psi(x)$. On the wall at $x_0 = 0$ we have

$$\begin{aligned} \mathbf{V}^\mu &= \frac{a^6}{L^3} \sum_{\mathbf{y}, \mathbf{z}} \bar{\zeta}(\mathbf{y}) \gamma^\mu \zeta(\mathbf{z}) \\ &= \frac{a^6}{L^3} \sum_{\mathbf{y}, \mathbf{z}} \bar{\psi}(0, \mathbf{y}) \frac{2\gamma^\mu - 2\gamma^0 g^{\mu 0} + [\gamma^0, \gamma^\mu]}{4} \psi(0, \mathbf{z}) \end{aligned} \quad (11)$$

Indeed the two boundary projectors act on γ^μ by killing its time component and by introducing a mixing with the tensor $\sigma^{0\mu} = i[\gamma^0, \gamma^\mu]/2$,

$$P_+ \gamma^\mu P_- = \begin{cases} 0, & \mu = 0 \\ \frac{1}{2}(\gamma^i - i\sigma^{0i}), & \mu = i = 1, 2, 3 \end{cases} \quad (12)$$

which, in compact notation, is equivalent to the gamma matrix combination appearing in eq. (11)

$$P_+ \gamma^\mu P_- = \frac{2\gamma^\mu - 2\gamma^0 g^{\mu 0} + [\gamma^0, \gamma^\mu]}{4} \quad (13)$$

The matrix elements of \mathbf{V}^μ between the vacuum and a vector meson state, entering the spectral decomposition of two and three point correlation functions, can be thus parametrized as

$$\langle 0 | \mathbf{V}^\mu | \mathcal{M}_V^\alpha \rangle = \rho_V [\epsilon_\alpha^\mu - \epsilon_\alpha^0 g^{0\mu}] + \rho_T [\epsilon_\alpha^\mu v_V^0 - \epsilon_\alpha^0 v_V^\mu] \quad (14)$$

The projection of the wall sources on the physical states entail unknown non-perturbative wave functions, ρ_V and ρ_T , that cancel out exactly in our choice of ratios of correlation functions discussed in the next subsection. Pseudoscalar mesons do not carry polarization indexes and the effect of the boundary conditions can be reabsorbed into a redefinition of the wave function,

$$\begin{aligned} \mathbf{P} &= \frac{a^6}{L^3} \sum_{\mathbf{y}, \mathbf{z}} \bar{\zeta}(\mathbf{y}) \gamma_5 \zeta(\mathbf{z}) \\ &= \frac{a^6}{L^3} \sum_{\mathbf{y}, \mathbf{z}} \bar{\psi}(0, \mathbf{y}) \frac{\gamma_5 + \gamma_0 \gamma_5}{2} \psi(0, \mathbf{z}) \end{aligned}$$

$$\begin{aligned} \langle 0 | \mathbf{P} | \mathcal{M}_P \rangle &= \rho_P + \rho_A v_P^0 \\ &= \tilde{\rho}_P \end{aligned} \quad (15)$$

The relations above hold at $x_0 = 0$ but the same arguments can be repeated for the boundary operators on the wall at $x_0 = T$ that in the following will be called \mathbf{P}' and \mathbf{V}'^μ .

For later use, we also define the improved bulk operators

$$\begin{aligned} \mathcal{A}^\mu(x_0) &= A^\mu(x) + a c_A \frac{\partial_\mu + \partial_\mu^*}{2} P(x) \\ \mathcal{V}^\mu(x) &= V^\mu(x) + a c_V \frac{\partial_\nu + \partial_\nu^*}{2} T^{\mu\nu}(x) \end{aligned} \quad (16)$$

where $P(x) = \bar{\psi}(x)\gamma_5\psi(x)$ is the pseudoscalar density, $A^\mu(x) = \bar{\psi}(x)\gamma^\mu\gamma_5\psi(x)$ the axial current and the improvement coefficients c_A and c_V have been taken from refs. [19, 20, 21].

B. Quark masses

Particle states are fixed by tuning the values of the corresponding quark masses. We use three definitions of renormalization group invariant quark masses differing at finite lattice spacing by terms of order $O(a^2)$. We have calculated the following two point correlation functions

$$\begin{aligned} f_{rr}^A(x_0) &= \sum_{\mathbf{x}} \langle \mathbf{P}_{rr} A_{rr}^0(x) \rangle \\ f_{rr}^P(x_0) &= - \sum_{\mathbf{x}} \langle \mathbf{P}_{rr} P_{rr}(x) \rangle \end{aligned} \quad (17)$$

and defined

$$am_r^{AWI} = \frac{1}{2f_{rr}^P} \left[\frac{\partial_0 + \partial_0^*}{2} f_{rr}^A + ac_A \partial_0 \partial_0^* f_{rr}^P \right] \quad (18)$$

$$am_r^b = \frac{1}{2} \left[\frac{1}{k_r} - \frac{1}{k_c} \right] \quad (19)$$

where a is the lattice spacing, k_r is the hopping parameter of the r quark and k_c is the critical value of the hopping parameter.

A first definition of renormalization group invariant (RGI) quark masses has been obtained by the following relation

$$m_r = Z_M [1 + (b_A - b_P) am_r^b] m_r^{AWI} \quad (20)$$

The combination $b_A - b_P$ of the improvement coefficients of the axial current and pseudoscalar density has been computed non-perturbatively in [22, 24]. The factor Z_M is known with very high precision in a range of inverse bare couplings that does not cover all the values of β used in our simulations. We have used the results reported in table 6 of ref. [23] to parametrize Z_M in the enlarged range of β values [5.9, 7.6]. A second definition of RGI quark mass has been obtained by the relation

$$m_r = Z_M Z [1 + b_m am_r^b] m_r^b \quad (21)$$

where the improvement coefficient b_m and the renormalization constant Z has been also taken from refs. [22, 24]. An additional definition of RGI quark masses has been obtained by using improved lattice derivatives in eq. (18).

C. Three point correlators

The matrix elements in eqs. (1) can be calculated on the lattice by building suitable ratios of the following

three point correlation functions

$$\begin{aligned} \langle PVP \rangle_{if}^\mu(x_0, \vec{p}_{P_i}, \vec{p}_{P_f}) &= Z_V^I \sum_{\vec{x}} \langle \mathbf{P}_{li} \mathcal{V}_{if}^\mu(x) \mathbf{P}'_{fl} \rangle \\ \langle VVV \rangle_{if}^{I\mu I} (x_0, \vec{p}_{V_i}, \vec{p}_{V_f}) &= Z_V^I \sum_{\vec{x}} \langle \mathbf{V}_{li}^I \mathcal{V}_{if}^\mu(x) \mathbf{V}'_{fl}^I \rangle \\ \langle PVV \rangle_{if}^{\mu I} (x_0, \vec{p}_{P_i}, \vec{p}_{V_f}) &= Z_V^I \sum_{\vec{x}} \langle \mathbf{P}_{li} \mathcal{V}_{if}^\mu(x) \mathbf{V}'_{fl}^I \rangle \\ \langle PAV \rangle_{if}^{\mu I} (x_0, \vec{p}_{P_i}, \vec{p}_{V_f}) &= Z_A^I \sum_{\vec{x}} \langle \mathbf{P}_{li} \mathcal{A}_{if}^\mu(x) \mathbf{V}'_{fl}^I \rangle \end{aligned} \quad (22)$$

In the previous equations we have explicitly indicated heavy (i, f) and light (l) flavor indices and we have implicitly defined

$$\begin{aligned} Z_V^I &= Z_V \left(1 + b_V \frac{am_i^b + am_f^b}{2} \right) \\ Z_A^I &= Z_A \left(1 + b_A \frac{am_i^b + am_f^b}{2} \right) \end{aligned} \quad (23)$$

Let us now consider the normalization factors

$$\begin{aligned} N_{if}^I(x_0, \vec{p}_{P_i}, \vec{p}_{V_f}) \\ = \sqrt{\langle PVP \rangle_{ii}^0(x_0, \vec{p}_{P_i}, \vec{p}_{P_i}) \langle VVV \rangle_{ff}^{I0I}(x_0, \vec{p}_{V_f}, \vec{p}_{V_f})} \end{aligned} \quad (24)$$

Because of our choice of spatial momenta (having non vanishing components along the direction $\hat{1}$ only) the normalization factors N^1 will in general be different from the remaining ones, $N^{2,3}$. By assuming single state dominance, by relying on the conservation of the vector current and by using the form factors definition, eqs. (1), and the completeness relation of the polarization vectors, eq. (2), we have

$$\begin{aligned} C^\perp &= \sqrt{v_P^0 v_V^0} \left\{ \frac{\langle PAV \rangle^{22}(T/2, \vec{p}_P, \vec{p}_V)}{N^2(T/2, \vec{p}_P, \vec{p}_V)} \right. \\ &\quad \left. + \frac{\langle PAV \rangle^{33}(T/2, \vec{p}_P, \vec{p}_V)}{N^3(T/2, \vec{p}_P, \vec{p}_V)} \right\} \\ &= (1 + w) h_{A_1} \\ B^\perp &= \sqrt{v_P^0 v_V^0} \left\{ \frac{\langle PVV \rangle^{32}(T/2, \vec{p}_P, \vec{p}_V)}{N^2(T/2, \vec{p}_P, \vec{p}_V)} \right. \\ &\quad \left. - \frac{\langle PVV \rangle^{23}(T/2, \vec{p}_P, \vec{p}_V)}{N^3(T/2, \vec{p}_P, \vec{p}_V)} \right\} \\ &= \sqrt{w^2 - 1} h_V \end{aligned} \quad (25)$$

The extraction of h_{A_1} from the first of the previous relations is straightforward. In view of the calculation of the decay rate (see eqs. (4), (6) and (7)), we do not remove the factor $\sqrt{w^2 - 1}$ from the second equation above. More precisely, we measure on the lattice the following combinations

$$h_{A_1} = \frac{\mathcal{C}^\perp}{1+w} \quad (26)$$

$$X_V = \sqrt{\frac{w-1}{w+1}} \frac{h_V}{h_{A_1}} = \frac{\mathcal{B}^\perp}{\mathcal{C}^\perp} \quad (27)$$

that enter directly the definition of $F^{B \rightarrow D^*}(w)$. In the case of the remaining form factors, h_{A_2} and h_{A_3} , we follow a similar path. By defining

$$\begin{aligned} \mathcal{C}^0 &= 2\sqrt{v_P^0 v_V^0} \frac{\langle PAV \rangle^{01}(T/2, \vec{p}_P, \vec{p}_V)}{N^1(T/2, \vec{p}_P, \vec{p}_V)} \\ &= (1+w)h_{A_1}v_V^1 + \sqrt{w^2 - 1} [h_{A_2}v_P^0 + h_{A_3}v_V^0] \\ \mathcal{C}^1 &= 2\sqrt{v_P^0 v_V^0} \frac{\langle PAV \rangle^{11}(T/2, \vec{p}_P, \vec{p}_V)}{N^1(T/2, \vec{p}_P, \vec{p}_V)} \\ &= (1+w)h_{A_1}v_V^0 + \sqrt{w^2 - 1} [h_{A_2}v_P^1 + h_{A_3}v_V^1] \end{aligned} \quad (28)$$

we measure on the lattice the following combinations of correlation functions

$$X_2 = (w-1) \frac{h_{A_2}}{h_{A_1}} = \frac{v_V^0 \mathcal{C}^1 - v_V^1 \mathcal{C}^0}{\mathcal{C}^\perp} - 1 \quad (29)$$

$$X_3 = (w-1) \frac{h_{A_3}}{h_{A_1}} = \frac{v_P^1 \mathcal{C}^0 - v_P^0 \mathcal{C}^1}{\mathcal{C}^\perp} + w \quad (30)$$

that provide the combinations of form factors entering the definition of $F^{B \rightarrow D^*}(w)$.

A key point in reducing statistical fluctuations in the extraction of the different combinations of form factors is the definition of the 4-velocities, and consequently of $w = v_P \cdot v_V$, entering eqs. (26), (29) and (30). A particularly convenient choice is the definition of velocities in terms of

three point correlation functions by the following ratios

$$\begin{aligned} \frac{p_{V_i}}{E_{V_i}} &= \frac{1}{3} \frac{\langle VVV \rangle_{ii}^{111}(T/2, \vec{p}_{V_i}, \vec{p}_{V_i})}{\langle VVV \rangle_{ii}^{101}(T/2, \vec{p}_{V_i}, \vec{p}_{V_i})} \\ &+ \frac{1}{3} \frac{\langle VVV \rangle_{ii}^{212}(T/2, \vec{p}_{V_i}, \vec{p}_{V_i})}{\langle VVV \rangle_{ii}^{202}(T/2, \vec{p}_{V_i}, \vec{p}_{V_i})} \\ &+ \frac{1}{3} \frac{\langle VVV \rangle_{ii}^{313}(T/2, \vec{p}_{V_i}, \vec{p}_{V_i})}{\langle VVV \rangle_{ii}^{303}(T/2, \vec{p}_{V_i}, \vec{p}_{V_i})} \end{aligned} \quad (31)$$

$$\frac{p_{P_i}}{E_{P_i}} = \frac{\langle PVP \rangle_{ii}^1(T/2, \vec{p}_{P_i}, \vec{p}_{P_i})}{\langle PVP \rangle_{ii}^0(T/2, \vec{p}_{P_i}, \vec{p}_{P_i})} \quad (32)$$

This way we have been able to define all the form factors entirely in terms of three point correlation functions and to keep under control statistical fluctuations also at non vanishing momentum transfer.

IV. THE STEP SCALING METHOD

The idea behind the SSM is to split the complexity of the calculation of quantities depending upon two largely separated energy scales into several calculations performed on different physical volumes. The small volume calculations are needed in order to resolve the dynamics of the heavy quarks without recurring to any approximation but introducing, at intermediate stages, finite volume effects (FVE)

$$\mathcal{O}(\text{physical}) = \mathcal{O}(\text{finite volume}) \times FVE \quad (33)$$

The finite volume effects are subsequently accounted for by performing simulations on progressively larger volumes. The success of this strategy depends on the details of the problem and hence on the possibility of computing the finite volume observable, finite volume effects and their product with smaller errors and systematics with respect to the ones that would be obtained by a direct calculation. The strength of the method is a great freedom in the definition of the observable on finite volumes provided that its physical value is recovered at the end of the procedure.

In the calculation of heavy-light meson observables the two scales are the mass of the heavy quarks (b, c) and the mass of the light quarks (u, d, s). Here we consider the form factor $F^{P \rightarrow V}(w)$ as a function of w , the volume, $L^3 \times T$, and identify heavy meson states by the corresponding RGI quark masses that in the infinite volume limit lead to the physical meson spectrum [9].

First we compute the observable $F^{B \rightarrow D^*}(w; L_0^3 \times L_0)$ on a small volume $L_0^3 \times L_0$, $T = L$, $L_0 \simeq 0.4$ fm, which is chosen to accommodate the dynamics of the b -quark. The observable on the finite volume is defined as explained in the previous section, i.e. by relying on single

state dominance of the different correlation functions. Of course this is not true at $x_0 = L_0/2 \simeq 0.2$ fm but, letting x_0 to scale proportionally to the volume in the finite size scaling iteration, becomes true by removing finite volume effects.

A first portion of finite volume effects is removed by evolving the volume from $L_0^3 \times L_0$ to $L_1^3 \times L_1$, $L_1 = 2L_0$, by the ratio

$$\sigma^{P \rightarrow D^*}(w; L_0, L_1) = \frac{F^{P \rightarrow D^*}(w; L_1^3 \times L_1)}{F^{P \rightarrow D^*}(w; L_0^3 \times L_0)} \quad (34)$$

The crucial point is that the step scaling functions are calculated by simulating heavy quark masses m_P smaller than the b -quark mass. The physical value $\sigma^{B \rightarrow D^*}(w; L_0, L_1)$ is obtained by a smooth extrapolation in $1/m_P$ that relies on the HQET expectations and upon the general idea that finite volume effects, measured by the σ 's, are almost insensitive to the high energy scale.

The final result is obtained by further evolving the volume from $L_1^3 \times L_1$ to $L_2^3 \times T_2$, with $L_2 = 4L_0$ and $T_2 = 3L_2/2$ by calculating a second step scaling function

$$\sigma^{P \rightarrow D^*}(w; L_1, L_2) = \frac{F^{P \rightarrow D^*}(w; L_2^3 \times 3L_2/2)}{F^{P \rightarrow D^*}(w; L_1^3 \times L_1)} \quad (35)$$

and by the following identity

$$\begin{aligned} F^{B \rightarrow D^*}(w; L_2^3 \times 3L_2/2) &= F^{B \rightarrow D^*}(w; L_0^3 \times L_0) \\ &\times \sigma^{B \rightarrow D^*}(w; L_0, L_1) \\ &\times \sigma^{B \rightarrow D^*}(w; L_1, L_2) \end{aligned} \quad (36)$$

V. LATTICE SIMULATIONS

A. Small volume

Simulations on the small volume $L_0^3 \times L_0$ have been carried out at three different values of the lattice spacing corresponding to the entries L_0A , L_0B and L_0C in TABLE I. The beta values have been deduced from refs [25, 26, 27] and have been matched by fixing the value of the renormalized strong coupling constant in the Schrödinger Functional scheme. The physical extension of the volume is $L_0 \simeq 0.718r_0$ where $r_0 \simeq 0.5$ fm [28].

On such a small volume we have simulated massless light quarks and we do not need to discuss the systematics associated to chiral extrapolations.

In FIG. 1 we show the continuum extrapolation of $F^{B \rightarrow D^*}(w; L_0^3 \times L_0)$ for the seven different values of w that have been simulated. Different fits correspond to the

	β	$L^3 \times T$	N_{cnfg}
L_0A	7.6547	$32^3 \times 32$	433
L_0B	7.4082	$24^3 \times 24$	298
L_0C	7.2611	$20^3 \times 20$	128
L_0a	7.0203	$16^3 \times 16$	293
L_0b	6.7750	$12^3 \times 12$	640
L_0c	6.4956	$8^3 \times 8$	1600
L_1A	7.0203	$32^3 \times 32$	326
L_1B	6.7750	$24^3 \times 24$	243
L_1C	6.4956	$16^3 \times 16$	120
L_1a	6.4956	$16^3 \times 16$	1051
L_1b	6.2885	$12^3 \times 12$	3168
L_1c	6.0219	$8^3 \times 8$	720
L_2A	6.4956	$32^3 \times 48$	152
L_2B	6.2885	$24^3 \times 36$	150
L_2C	6.0219	$16^3 \times 24$	200

TABLE I: Table of lattice simulations.

three different definitions of quark masses introduced in section III: the extrapolations must coincide within the errors as happens to be in practice and the continuum results are defined by a jackknife average. In general we combine results of different simulations in big jackknife samples according to the recipe discussed in the Appendix A of ref. [29].

In FIG. 2 we show the different form factors that enter into the definition of $F^{B \rightarrow D^*}(w; L_0^3 \times L_0)$ already extrapolated to the continuum limit. As expected, $X_V(w)$, $X_2(w)$ and $X_3(w)$ vanish at zero recoil while $h_{A_1}(w)$ is of order one. The scale of the figure does not allow to distinguish the errors that are much smaller than the symbols but it allows to appreciate the relative sizes of the different form factors.

Concerning the renormalization factors, our definitions of $h_{A_1}(w)$ and $X_V(w)$ require the knowledge of Z_A/Z_V and of $(b_A - b_V)$ while, in the case of $X_2(w)$ and $X_3(w)$, these cancel out in the ratios. Unfortunately the ratio Z_A/Z_V has not been computed directly and we have used the separate non-perturbative determinations of Z_A and Z_V performed in ref. [30]. Also b_V has been non-perturbatively determined in ref. [30] while for b_A we use its perturbative value (approximation well justified at this small values of bare couplings and, a posteriori, by looking at the continuum extrapolations of FIG. 1). The overall systematics due to renormalization factors is largely accounted for by adding a 0.6% relative error to our final result (see ref. [30]). Since renormalization factors cancel out in the definition of the step scaling functions there are no other systematics associated to the renormalization procedure in our calculation.

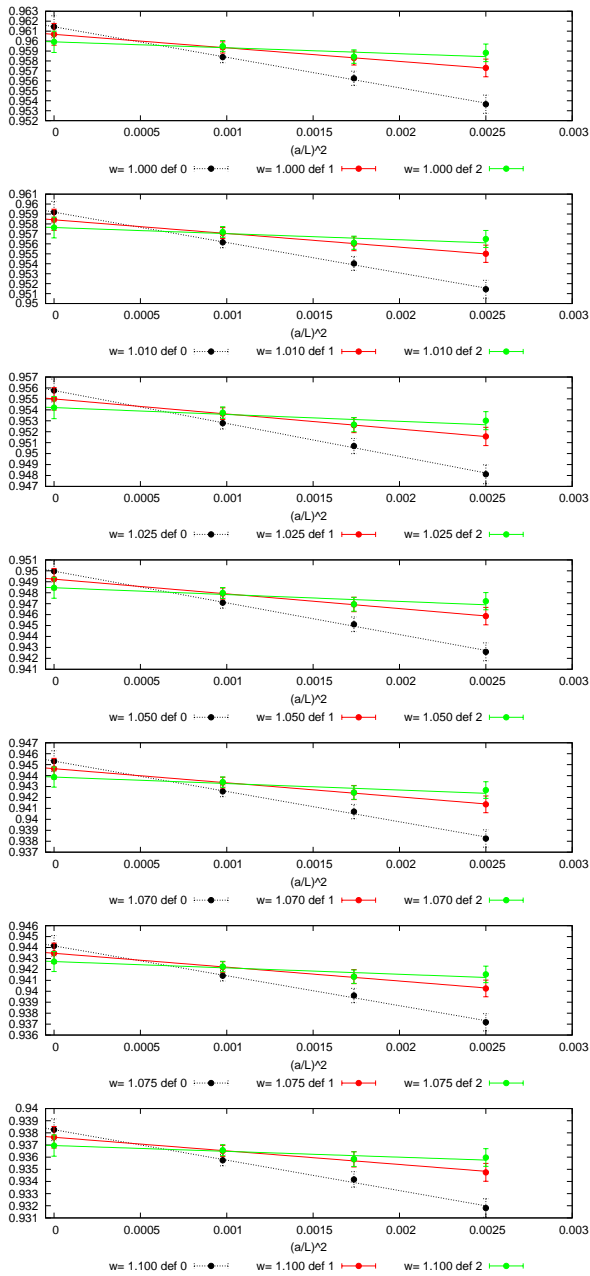


FIG. 1: Continuum extrapolations of $F^{B \rightarrow D^*}(w; L_0^3 \times L_0)$ for the different simulated values of w . The different fits are linear in $(a/L_0)^2$ and correspond to different definitions of RGI quark masses.

B. Intermediate volume

The step toward the intermediate volume $L_1^3 \times L_1$, $L_1 = 2L_0$, has been performed by calculating the denominator of eq. (34) at three different lattice spacings, corresponding to the entries L_0a , L_0b and L_0c of TABLE I, and the numerator with the same lattice spacings but with twice the number of lattice points per direction, entries L_1A , L_1B and L_1C of TABLE I. Also for

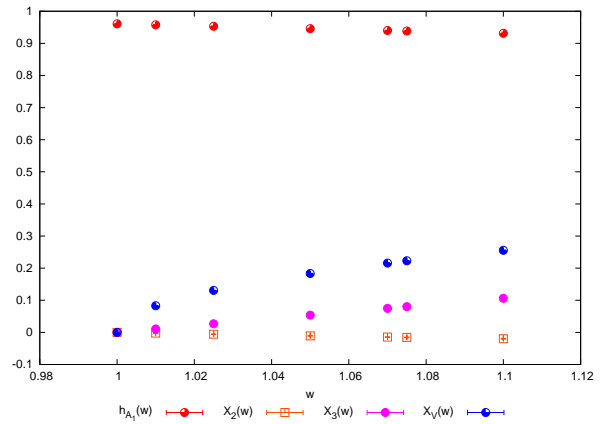


FIG. 2: Small volume results for $h_{A_1}(w)$, $X_V(w)$, $X_2(w)$ and $X_3(w)$. On this scale the errors are much smaller than the symbols.

this step the light quark has been simulated at zero mass. The value of the heaviest quark mass simulated on these volumes has been halved with respect to the previous step in order to have the same order of cutoff effects.

In FIG. 3 we show the continuum extrapolation of $\sigma^{P \rightarrow D^*}(w; L_0, L_1)$ for the seven different values of w that have been simulated. The pseudoscalar meson state correspond to a quark having a mass of about half of the physical value of the b -quark mass ($m_P \simeq m_b/2$) i.e. the heaviest mass simulated on these volumes; similar plots could have been shown for the other simulated heavy quark masses. Different fits correspond to the three different definitions of quark masses introduced in section III: the continuum results are defined by the jack-knife average of the independent extrapolations.

In FIG. 4 we can test our hypothesis of the low sensitivity of the finite volume effects upon the heavy quark mass. The figure shows the step scaling function $\sigma^{P \rightarrow D^*}(w; L_0, L_1)$ in the continuum limit and at fixed w as a function of the inverse RGI heavy quark mass of the pseudoscalar state $1/m_P$. The RGI heavy quark mass of the vector state has been held fixed to its physical value m_c . The physical step scaling functions are obtained by linear extrapolations so mild that the values at m_b differ by the simulated ones by a few per mille.

C. Final volume

The last step of the finite size scaling procedure has been performed by calculating the denominator of eq. (35) at three different lattice spacings, corresponding to the entries L_1a , L_1b and L_1c of TABLE I, and the numerator with the same lattice spacings but with twice the number of lattice points along the spatial directions and three times the number of points along the time direction, entries L_2A , L_2B and L_2C of TABLE I. The choice

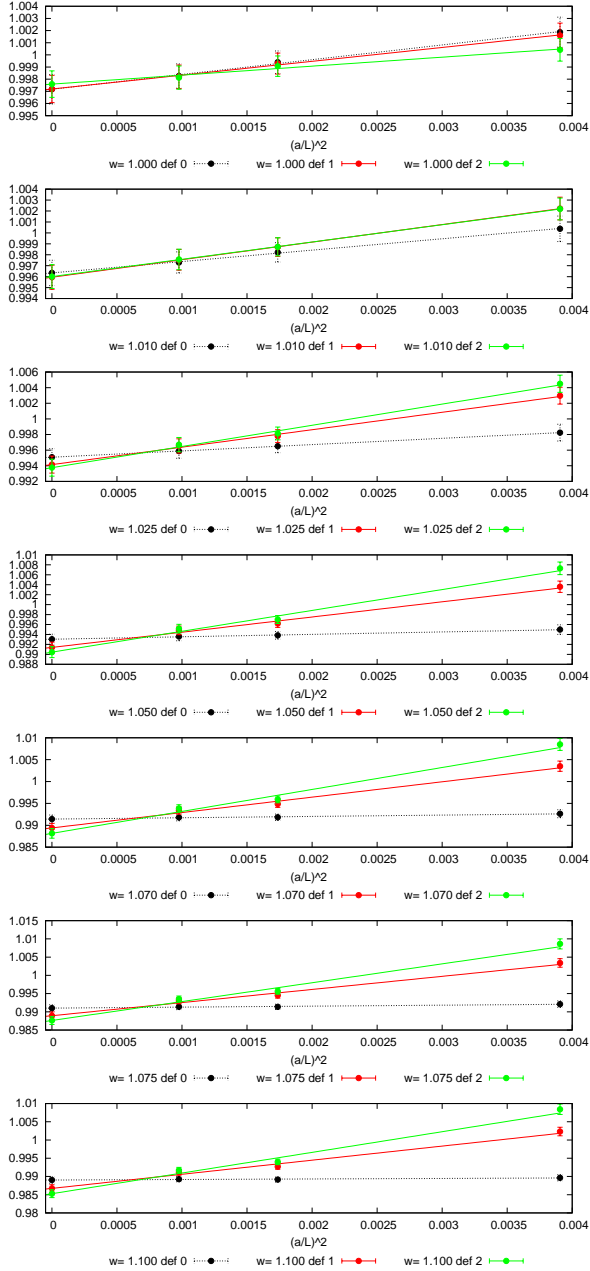


FIG. 3: Continuum extrapolations of $\sigma^{P \rightarrow D^*}(w; L_0, L_1)$ for the heaviest quark mass ($m_P \simeq m_b/2$) simulated on this step and for the different simulated values of w . The different fits are linear in $(a/L_0)^2$ and correspond to different definitions of RGI quark masses.

of $T = 3L/2$ in the numerator of the last step is motivated by the need of reaching a time extent in physical units that justifies the single state dominance hypothesis. This can also be compared with the different sequence of steps, carried out in our previous papers [5, 6], reaching the same final time extent.

In FIG. 5 we show the continuum extrapolation of $\sigma^{P \rightarrow D^*}(w; L_1, L_2)$ for the seven different values of w that

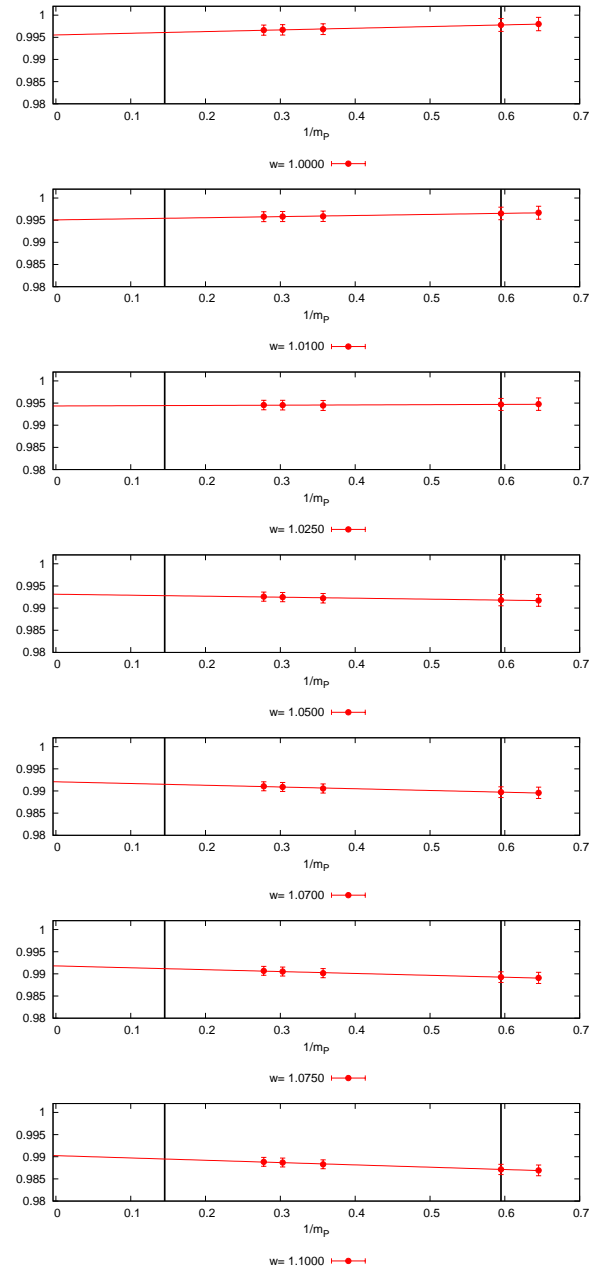


FIG. 4: Continuum step scaling function $\sigma^{P \rightarrow D^*}(w; L_0, L_1)$ as a function of the inverse RGI heavy quark mass of the pseudoscalar state, $1/m_P$, for the different values of w . The vertical black lines represent the physical values of the charm and bottom quark masses.

have been simulated. The pseudoscalar meson state correspond to a heavy quark having a mass of about a quarter of the physical value of the b -quark mass ($m_P \simeq m_b/4$), the heaviest mass simulated on these volumes; similar plots could have been shown for the other simulated heavy quark masses. In this step we have used a single definition of RGI quark masses and precisely the one of eq. (20).

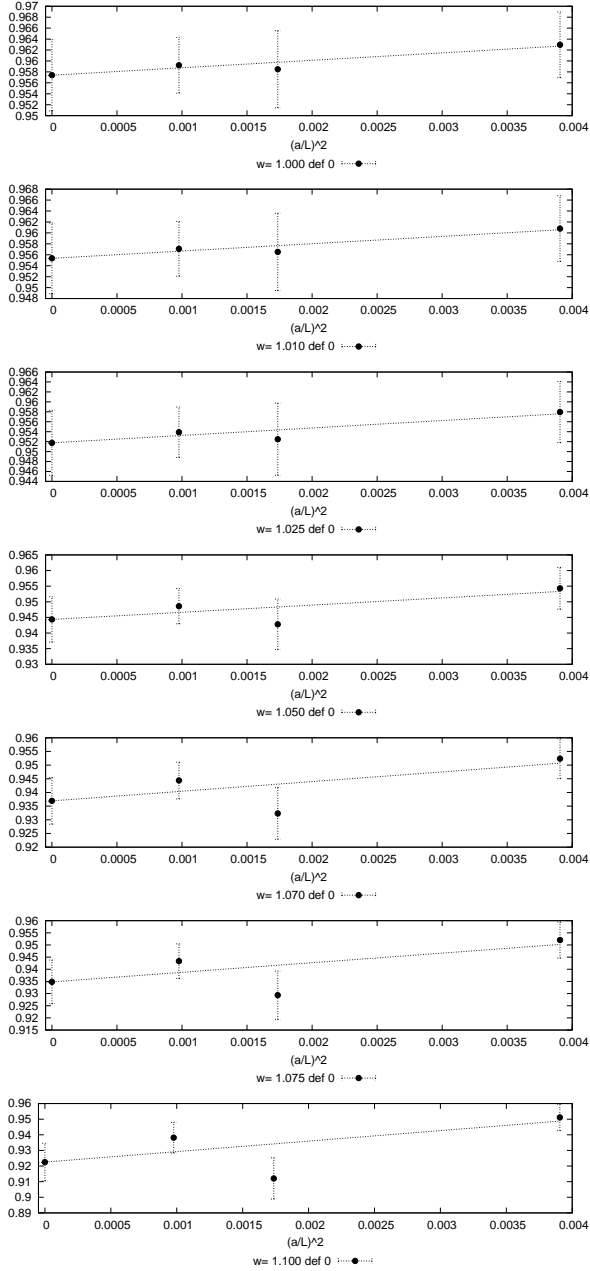


FIG. 5: Continuum extrapolations of $\sigma^{P \rightarrow D^*}(w; L_1, L_2)$ for the heaviest quark mass ($m_P \simeq m_b/4$) simulated on this step, $m_l = m_s$ and for the different simulated values of w .

In FIG. 6 we show the extrapolations of the continuum step scaling function $\sigma^{P \rightarrow D^*}(w; L_1, L_2)$ to the physical point. The RGI heavy quark mass of the vector state has been held fixed to its physical value m_c . Also in this second step the dependence of the finite volume effects upon the heavy quark mass of the pseudoscalar state is very mild. The fact that we measure larger finite volume effects with respect to the ones obtained on the previous step can be explained by assuming that these are mainly due to the contribution of excited states to the correlation functions entering the definition of the lattice matrix

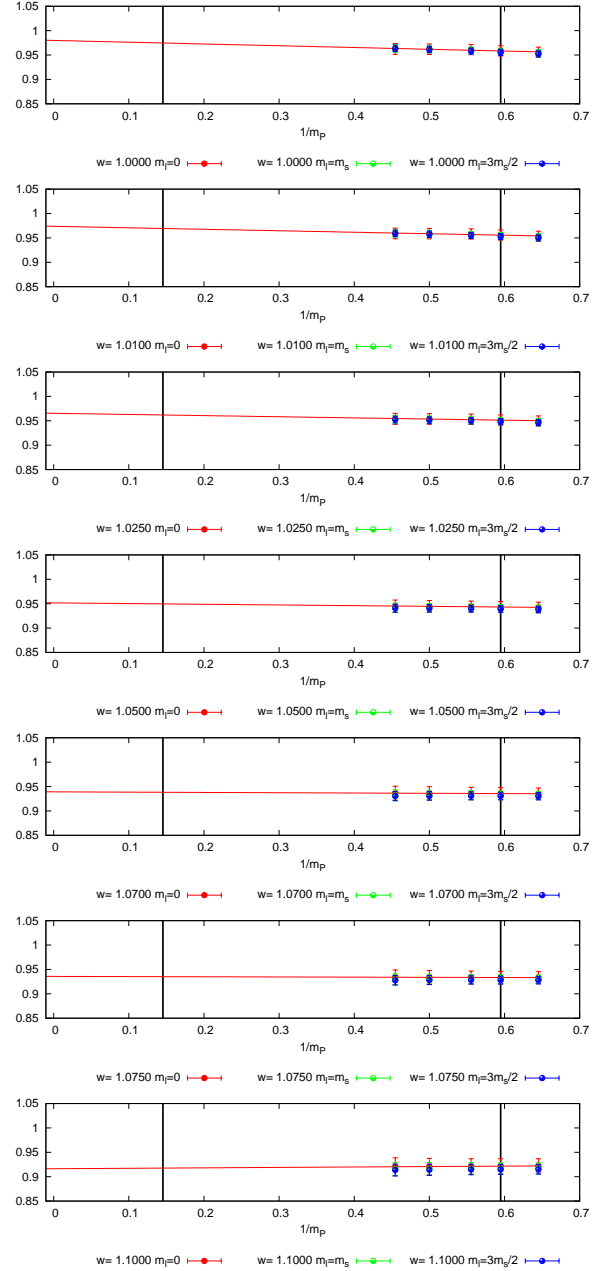


FIG. 6: Continuum step scaling function $\sigma^{P \rightarrow D^*}(w; L_1, L_2)$ as a function of the inverse RGI heavy quark mass of the pseudoscalar state, $1/m_P$, for the different values of w . The vertical black lines represent the physical values of the charm and bottom quark masses. Symbols of different colors correspond to different values of the light quark mass.

elements rather than to the matrix elements themselves. Indeed, in passing from the denominator to the numerator of eq. (35) the time extent of the final volume is enlarged of a factor three, $T_2 \simeq 2.4$ fm. The validity of this hypothesis is supported by the results of a series of simulations of the volume $L_2^3 \times L_2$ not shown in this paper.

w	$F^{B \rightarrow D^*}(w)$	$\frac{F^{B \rightarrow D^*}(w)}{G^{B \rightarrow D}(w)}$	N_f	reference
1.000	0.917(08)(05)	0.878(10)(04)	0	this work
1.010	0.913(09)(05)	0.883(09)(04)	0	this work
1.025	0.905(10)(05)	0.891(09)(04)	0	this work
1.050	0.892(13)(04)	0.905(10)(04)	0	this work
1.070	0.880(17)(04)	0.914(12)(05)	0	this work
1.075	0.877(18)(04)	0.916(12)(05)	0	this work
1.100	0.861(23)(04)	0.923(16)(05)	0	this work
1.00	0.913(20)(16)		0	[16]
1.00	0.924(12)(19)		2+1	[15]

TABLE II: Final results in the continuum and infinite volume limits. As a comparison we quote also the results of previous lattice calculations of $F^{B \rightarrow D^*}(w)$ by the Fermilab collaboration.

It has not been possible to simulate light quarks at vanishing mass on the final volume and we have computed the step scaling function $\sigma^{P \rightarrow D^*}(w; L_1, L_2)$ at three different values of m_l ranging from about $3m_s/2$ to about m_s , the physical value of the strange quark mass. Symbols of different colors in the plots of FIG. 6 show the step scaling functions for different values of m_l . We do not see any appreciable dependence of finite volume effects upon m_l within the statistical errors and obtain results in the chiral limit by a linear fit. The slopes of these fits are at least an order of magnitude smaller than their error.

VI. COMPARISON WITH EXPERIMENT

Our final results for $F^{B \rightarrow D^*}(w)$ are obtained by multiplying the small volume numbers with the two step scaling functions according to eq. (36) and are shown in TABLE II. The first error is statistical while the second comes from the uncertainties associated to the renormalization factors on the small volume (see discussion in section II). As a comparison we quote in table TABLE II the results of previous lattice calculations obtained by the Fermilab lattice collaboration [15, 16] at zero recoil.

FIG. 7 shows the comparison of our lattice data with some experimental determinations of $|V_{cb} \times 10^3| F^{B \rightarrow D^*}(w)$ [31, 32, 33, 34]: the functional dependence of experimental data upon w is reproduced by lattice data within statistical errors also in the quenched approximation. The comparison is made by matching lattice data with the experimental ones from ref. [31] at $w = 1.075$ and by obtaining

$$|V_{cb}| = 3.74(8)(5) \times 10^{-2} \quad (37)$$

where the first error is from theory while the second from experiment. This number is in good agreement with our previous determination of the CKM matrix element, $V_{cb} = 3.84(9)(42) \times 10^{-2}$, performed in ref. [5] by

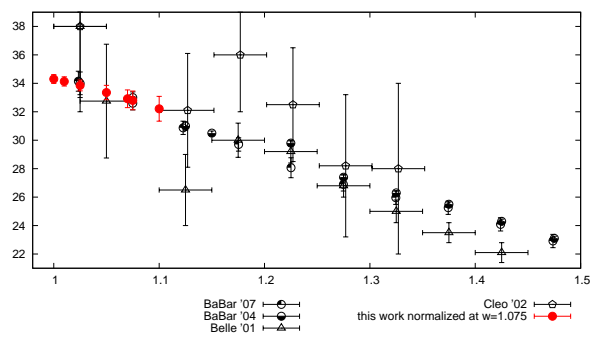


FIG. 7: Comparison of $|V_{cb} \times 10^3| F^{B \rightarrow D^*}(w)$ obtained in this work with experimental data. Lattice data carry only statistical errors and are normalized at $w = 1.075$.

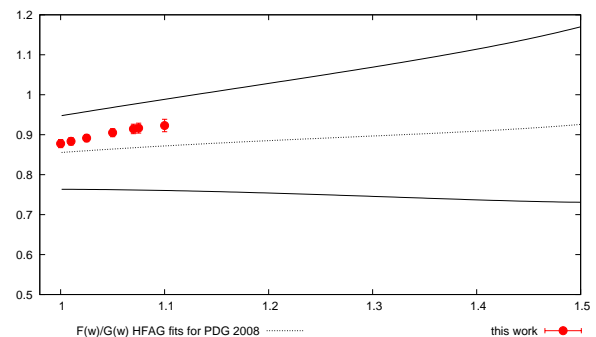


FIG. 8: Comparison of the ratio $F^{B \rightarrow D^*}(w)/G^{B \rightarrow D}(w)$ obtained in this work with the fits to experimental data performed by the HFAG for the 2008 edition of the PDG. Lattice data carry only statistical errors.

matching $G^{B \rightarrow D}(w)$, the form factor entering the decay rate of the process $B \rightarrow D \ell \nu$, with experimental data at $w = 1.2$. In both the cases V_{cb} has been extracted at non vanishing momentum transfer and the corresponding uncertainties are not correlated with the errors on the parameters of the fits needed to extrapolate measured decay rates to zero recoil.

A more direct comparison between lattice and experiment can be obtained by introducing the ratio $F^{B \rightarrow D^*}(w)/G^{B \rightarrow D}(w)$ that does not depend upon V_{cb} . In order to apply a jackknife procedure directly to the ratio of the two form factors, we have computed $G^{B \rightarrow D}(w)$ on the same gauge ensembles of $F^{B \rightarrow D^*}(w)$ by following the finite size scaling recursion described in section IV and by using the definition of $G^{B \rightarrow D}(w)$ discussed in refs. [5, 6]. Our results are given in TABLE II and compared with experiment in FIG. 8. The black curves have been drawn by using the two independent fits¹ of the experimental data for $F^{B \rightarrow D^*}(w)$ and for $G^{B \rightarrow D}(w)$ per-

¹ A direct evaluation from the experimental collaborations of the ratio of decay rates would likely lead to a more stringent test.

formed by the Heavy Flavour Averaging Group [35] by using the parametrizations of ref. [36]. Our results, red points in the figure, fall inside the allowed experimental region, i.e. between the two solid black curves. Theoretical errors are smaller than experimental ones that in turn are dominated by the uncertainties on $G^{B \rightarrow D}(w)$. Also from this parameter-free comparison with experiments we obtain a strong indication for the validity of the quenched approximation for these observables. Together with the evidence of mild volume effects (if we exclude those coming from excited states contributions to correlation functions) these results may call for a basic short distance nature of the form factors. This could justify why main unquenching effects are reabsorbed by the

renormalization procedure of the quenched calculation that fixes indirectly the renormalized coupling constant from physical quantities.

Acknowledgments

We warmly thank R. Faccini and F. Cossutti for providing us the data of figure 6 of ref. [31]. The simulations required to carry on this project have been performed on the INFN apeNEXT machines at Rome "La Sapienza". We thank A. Lonardo, D. Rossetti and P. Vicini for technical advice.

-
- [1] N. Cabibbo, Phys. Rev. Lett. **10** (1963) 531.
 [2] M. Kobayashi and T. Maskawa, Prog. Theor. Phys. **49** (1973) 652.
 [3] M. Bona *et al.* [UTfit Collaboration], arXiv:0803.0659 [hep-ph].
 [4] M. Bona *et al.* [UTfit Collaboration], JHEP **0610** (2006) 081 [arXiv:hep-ph/0606167].
 [5] G. M. de Divitiis, E. Molinaro, R. Petronzio and N. Tantalo, Phys. Lett. B **655** (2007) 45 [arXiv:0707.0582 [hep-lat]].
 [6] G. M. de Divitiis, R. Petronzio and N. Tantalo, JHEP **0710** (2007) 062 [arXiv:0707.0587 [hep-lat]].
 [7] M. Guagnelli, F. Palombi, R. Petronzio and N. Tantalo, Phys. Lett. B **546** (2002) 237 [arXiv:hep-lat/0206023].
 [8] G. M. de Divitiis, M. Guagnelli, F. Palombi, R. Petronzio and N. Tantalo, Nucl. Phys. B **672**, 372 (2003) [arXiv:hep-lat/0307005].
 [9] G. M. de Divitiis, M. Guagnelli, R. Petronzio, N. Tantalo and F. Palombi, Nucl. Phys. B **675**, 309 (2003) [arXiv:hep-lat/0305018].
 [10] D. Guazzini, R. Sommer and N. Tantalo, JHEP **0801** (2008) 076 [arXiv:0710.2229 [hep-lat]].
 [11] G. M. de Divitiis, R. Petronzio and N. Tantalo, Phys. Lett. B **595**, 408 (2004) [arXiv:hep-lat/0405002].
 [12] P. F. Bedaque, Phys. Lett. B **593** (2004) 82 [arXiv:nucl-th/0402051].
 [13] C. T. Sachrajda and G. Villadoro, Phys. Lett. B **609**, 73 (2005) [arXiv:hep-lat/0411033].
 [14] J. M. Flynn, A. Juttner and C. T. Sachrajda [UKQCD Collaboration], Phys. Lett. B **632**, 313 (2006) [arXiv:hep-lat/0506016].
 [15] J. Laiho [Fermilab Lattice and MILC Collaborations], PoS **LATTICE2007** (2006) 358 [arXiv:0710.1111 [hep-lat]].
 [16] S. Hashimoto, A. S. Kronfeld, P. B. Mackenzie, S. M. Ryan and J. N. Simone, Phys. Rev. D **66** (2002) 014503 [arXiv:hep-ph/0110253].
 [17] M. Luscher, R. Narayanan, P. Weisz and U. Wolff, Nucl. Phys. B **384** (1992) 168 [arXiv:hep-lat/9207009].
 [18] S. Sint, Nucl. Phys. B **421**, 135 (1994) [arXiv:hep-lat/9312079].
 [19] M. Luscher, S. Sint, R. Sommer, P. Weisz and U. Wolff, Nucl. Phys. B **491** (1997) 323 [arXiv:hep-lat/9609035].
 [20] M. Guagnelli and R. Sommer, Nucl. Phys. Proc. Suppl. **63**, 886 (1998) [arXiv:hep-lat/9709088].
 [21] S. Sint and P. Weisz, Nucl. Phys. B **502**, 251 (1997) [arXiv:hep-lat/9704001].
 [22] G. M. de Divitiis and R. Petronzio, Phys. Lett. B **419** (1998) 311 [arXiv:hep-lat/9710071].
 [23] S. Capitani, M. Luscher, R. Sommer and H. Wittig [ALPHA Collaboration], Nucl. Phys. B **544** (1999) 669 [arXiv:hep-lat/9810063].
 [24] M. Guagnelli, R. Petronzio, J. Rolf, S. Sint, R. Sommer and U. Wolff [ALPHA Collaboration], Nucl. Phys. B **595**, 44 (2001) [arXiv:hep-lat/0009021].
 [25] M. Della Morte, N. Garron, M. Papinutto and R. Sommer, JHEP **0701** (2007) 007 [arXiv:hep-ph/0609294].
 [26] M. Della Morte, A. Shindler and R. Sommer, JHEP **0508**, 051 (2005) [arXiv:hep-lat/0506008].
 [27] J. Heitger and J. Wennekers [ALPHA Collaboration], JHEP **0402**, 064 (2004) [arXiv:hep-lat/0312016].
 [28] R. Sommer, Nucl. Phys. B **411** (1994) 839 [arXiv:hep-lat/9310022].
 [29] L. Del Debbio, L. Giusti, M. Luscher, R. Petronzio and N. Tantalo, JHEP **0702** (2007) 082 [arXiv:hep-lat/0701009].
 [30] M. Luscher, S. Sint, R. Sommer and H. Wittig, Nucl. Phys. B **491** (1997) 344 [arXiv:hep-lat/9611015].
 [31] B. Aubert *et al.* [BABAR Collaboration], Phys. Rev. D **77** (2008) 032002 [arXiv:0705.4008 [hep-ex]].
 [32] B. Aubert *et al.* [BABAR Collaboration], Phys. Rev. D **71** (2005) 051502 [arXiv:hep-ex/0408027].
 [33] R. A. Briere *et al.* [CLEO Collaboration], Phys. Rev. Lett. **89**, 081803 (2002) [arXiv:hep-ex/0203032].
 [34] K. Abe *et al.* [BELLE Collaboration], Phys. Lett. B **526**, 247 (2002) [arXiv:hep-ex/0111060].
 [35] E. Barberio *et al.* [Heavy Flavor Averaging Group (HFAG) Collaboration], arXiv:0704.3575 [hep-ex]. <http://www.slac.stanford.edu/xorg/hfag>.
 [36] I. Caprini, L. Lellouch and M. Neubert, Nucl. Phys. B **530** (1998) 153 [arXiv:hep-ph/9712417].